Growth of Phthalocyanine Doped and Undoped Nanotubes Using Mild Synthesis Conditions for Development of Novel Oxygen Reduction Catalysts

Robert L. Arechederra,[†] Kateryna Artyushkova,[‡] Plamen Atanassov,[‡] and Shelley D. Minteer*,[†]

Department of Chemistry, Saint Louis University, 3501 Laclede Avenue, St. Louis, Missouri 63103, United States, and Department of Chemical and Nuclear Engineering, The University of New Mexico, 1 University of New Mexico, Albuquerque, New Mexico 87131, United States

ABSTRACT Precious metal alloys have been the predominant electrocatalyst used for oxygen reduction in fuel cells since the 1960s. Although performance of these catalysts is high, they do have drawbacks. The two main problems with precious metal alloys are catalyst passivation and cost. This is why new novel catalysts are being developed and employed for oxygen reduction. This paper details the low temperature solvothermal synthesis and characterization of carbon nanotubes that have been doped with both iron and cobalt centered phthalocyanine. The synthesis is a novel low-temperature, supercritical solvent synthesis that reduces halocarbons to form a metal chloride byproduct and carbon nanotubes. Perchlorinated phthalocyanine was added to the nanotube synthesis to incorporate the phthalocyanine structure into the graphene sheets of the nanotubes to produce doped nanotubes that have the catalytic oxygen reduction capabilities of the metallo-phthalocyanine and the advantageous material qualities of carbon nanotubes. The cobalt phthalocyanine doped carbon nanotubes showed a half wave oxygen reduction potential of −0.050 ± 0.005 V vs Hg\HgO, in comparison to platinum's half wave oxygen reduction potential of −0.197 ± 0.002 V vs Hg\HgO.

KEYWORDS: fuel cells • oxygen reduction • rotating disk electrochemistry • carbon nanotubes • phthalocyanine

INTRODUCTION

Platinum and its alloys have been the electrochemical standard for oxygen reduction, but these metals are not ideal for fuel cell applications, because of their high cost, nonrenewability, passivation, and stability problems (1, 2). Platinum, like other precious metals, is of limited quantity on the earth, so the cost is high and the availability is low (3, 4). This is one of the major hurdles that has kept fuel cells from becoming mainstream in the market. Another major issue is that once the platinum catalyst is exposed to trace fuel impurities or air pollutants such as carbon monoxide or organic chemical vapors, the catalytic surface of the platinum passivates making it unable to further catalyze the necessary reactions. Alloys of platinum with other metals such as cobalt, ruthenium, iron, and tin have been created that help maintain the catalytic ability and allow for more tolerance of these catalyst poisons, but these catalysts still contain a large amount of costly precious metal (1, 2, 4−8).

In an effort to mimic the highly efficient oxygen reduction in biological systems, some researchers have been exploring porphyrin and phthalocyanine metal chelates which are very commonly observed as oxygen transporters and sites of oxygen reduction within cells (9−15). For example, cytochrome c oxidase, which contains a porphyrin macrocycle ring with an iron atom chelated at its center, is the catalyst for oxygen reduction in the outer membrane of mitochondria. While cytochrome c oxidase works well for mitochondria, its performance ex vivo immobilized on an electrode cannot compare with the performance of a precious metal catalyst (14). There are many reasons why this biomimic lacks performance, one major reason is that it is no longer in a lipid membrane so the orientation and stability of the enzyme is not as controllable. The other reason is that it does not have the proper interface to the carbon electrode material, so it cannot accept electrons efficiently. This is why several research groups have been focused on engineering a porphyrin or metal chelate catalyst into a good material that can interact efficiently with an electrode (16).

Some success of demonstrating catalytic ability has been achieved with intercalating the planar porphyrin or phthalocyanine into basal plane graphite, but the low surface area of basal plane graphite lacks high current densities and basal plane graphite is expensive making it not an ideal choice for a fuel cell electrode material (17). The most successful porphyrin-based oxygen reduction catalyst, which can be directly compared to platinum, has been a pyropolymer made by pyrolyzing a cobalt porphyrin (18). This type of material maintains the same catalytic chemistry as the parent compound, but is a more easily engineered material

* Corresponding author. Phone: (314) 977-3624. Fax: (314)-977-2521. E-mail: minteers@slu.edu.
Received for review August 12, 2010 and accepted October 21, 2010
[†] Saint Louis University.
[‡] The University of New Mexico.
DOI: 10.1021/am100724v

that can be used in a fuel cell. It does not poison in the presence of methanol and has good carbon monoxide tolerance (17−20). It also has the capability to reduce oxygen in both acidic and basic media which is a rare amphoteric catalytic phenomenon shared mostly by noble metal catalysts, because the reaction mechanism is different for each media (17−21). The main setback with this pyropolymer is while it interacts with the electrode much better than the parent porphyrin, it is still difficult to fabricate (17, 19−21). In an effort to make an easily fabricated material while still maintaining the same catalytic properties, effort has been focused in this work to incorporate iron and cobalt phthalocyanines into the growing graphene sheets during the synthesis of carbon nanotubes. Carbon nanotubes are typically produced by chemical vapor deposition of ethylene, acetylene or similar hydrocarbon gas, but have also been synthesized in supercritical solvents such as toluene at extreme temperatures and pressures (22−24). In both cases, the synthesis of the nanotubes is not as practical as with other materials such as carbon black mainly because the equipment used is expensive and difficult to scale. This is why to begin this work a low-temperature, low-pressure synthesis of carbon nanotubes was necessary to develop. It is well-known that carbon halides are highly reactive with the alkali metals, because the halide oxidizes the metal very exothermically, using this logic several experiments were developed that reduced carbon tetrahalides with metal powders. To compliment the reduction of the carbon, the reaction was done in a solvent at its critical point. The solvent chosen was hexane, because it has a critical temperature of 235 °C at 440 psi and at the synthesis temperature of 250 °C, it had a calculated vapor pressure of 500 psi. At these temperatures and pressures, solvent choice is nontrivial and complicated, because side reaction can begin to occur. Hexane is still mostly unreactive under these reaction conditions. Acetone has a similar critical point at 235 °C with higher pressure (680 psi) and a calculated vapor pressure of 870 psi at 250 °C, but while having the optimal temperature and pressure range, it undergoes unwanted side reactions when halogens are present.

EXPERIMENTAL SECTION

Materials. Iron hexadecachlorophthalocyanine (Sigma), sodium nitrate (Sigma), potassium hydroxide (Sigma), sodium borohydride (Sigma), carbon tetrachloride (Sigma), cobaltocene (Sigma), iron powder (Sigma), hexane (Sigma), nitric acid (Sigma), hydrochloric acid (Sigma), hexane (Sigma), ethanol (Sigma), methanol (Sigma), tetrabutylammonium bromide (Sigma), and Nafion 1100EW suspension (Aldrich) were used as received.

Low-Temperature Synthesis of Carbon Nanotubes. For the synthesis, a Parr acid digestion bomb was used that had a 23 mL Teflon cup and lid as the reaction container and the vessel was sealed. To the cup, 4.5 g of iron powder was added along with 0.25 g of carbon tetrachloride and 5 mL of hexane. The vessel was sealed and placed into a convection oven set at 250 °C for 24 h. In another experiment, an additional carbon nanotube growth catalyst was used. In this experiment, an additional 80 mg of cobaltocene was added to the reaction mixture, then allowed to react in the bomb at 250 °C for 24 h. Then the acid digestion bomb was removed from the oven and placed in the fume hood to cool for 2 h. Once at room temperature, the vessel was opened and the contents was poured/scraped into a beaker where 50 mL of a mixture of 50% concentrated nitric acid and 50% concentrated hydrochloric acid (aqua regia) by volume was added and allowed to digest the unreacted metal powder. When the solution stopped producing bubbles, it and the black precipitate was poured into a centrifuge tube and centrifuged at 5000Xg for 15 min. The yellow supernatant was discarded and 50 mL of aqua regia was added to the black precipitate in the centrifuge tube. The tube was shaken to resuspend the precipitate and let sit uncapped to further dissolve any further metal powder that remained for 15 min. Then it was centrifuged again at 5000Xg for 15 min and the supernatant was discarded. This step of rinsing the black precipitate with aqua regia was repeated three more times to ensure all of the metal powder was completely dissolved. The black precipitate was then rinsed five times with deionized water in the same manner as with the aqua regia to ensure any metal salt that formed or remaining acid was washed away. Once thoroughly washed, the black precipitate was rinsed in the same manner, but with methanol four times to remove the remaining water and any organic residues. The centrifuge tube containing the moist black precipitate was then placed into a vacuum desiccator overnight to dry. The next morning, the dry precipitate was placed into a sealed vial until further use.

Low-Temperature Synthesis of Phthalocyanine Doped Carbon Nanotubes. For the synthesis, a Parr acid digestion bomb was used that had a 23 mL Teflon cup and lid where the reactants were placed and the vessel was sealed. To the cup was added 1.0 g of iron powder along with 0.50 g of carbon tetrachloride, 0.364 g of iron hexadecachlorophthalocyanine, and 5 mL of hexane. The vessel was sealed and placed into a convection oven set at 250 °C for 24 h, and followed by the same cleaning, rinsing, and centrifuging procedure detailed previously.

Replacing the Chelated Iron with Cobalt. Iron phthalocyanine doped nanotubes (Fe-PNTs) that were synthesized previously and cleaned were used for the metal exchange procedure. Fifty milligrams of Fe-PNT was added into a nickel crucible with lid. To the crucible was then added 2.0 g of cobalt chloride hexahydrate. The Fe-PNTs and the cobalt chloride crystals were mixed together with a spatula and the crucible was covered with its lid. The crucible was then heated strongly on the bottom with a propane torch until it glowed orange for 5 min. Then the heat was removed and the crucible was allowed to return to room temperature. Once cool, the solidified contents (blackish-blue solid with metallic flakes) was chipped out of the bottom of the crucible with a spatula and placed into a centrifuge tube with 50 mL of concentrated nitric acid and allowed to dissolve the metal flakes and solidified cobalt chloride. Once the solution stopped bubbling and the solid lumps were dissolved, the contents were centrifuged at 5000 × g for 15 min and the pink supernatant was discarded. The black precipitate on the bottom was then rinsed by repeating the procedure two more times with concentrated nitric acid. Next, the black precipitate was rinsed by adding 50 mLof distilled water into the centrifuge tube and shaking to resuspend the precipitate. It was then centrifuged again at 5000 × g for 15 min and the supernatant was discarded. This distilled water rinsing procedure was repeated a minimum of 3 times or until the supernatant was uncolored. The final rinsing involved adding 50 mL of methanol to the black precipitate to wash any organic residues away, shaking to resuspend, and centrifuging at 5000 × g for 15 min. This final rinsing procedure was repeated 3 times and the black precipitate was then allowed to dry in a vacuum desiccator overnight. The next morning the dry precipitate was placed into a vial to await further use.

Electrochemical Characterization of Doped Nanotubes. Rotating disk electrode and rotating ring disk electrode volta-

mmetry was used to characterize the oxygen reduction of the doped nanotubes. To prepare the glassy carbon rotating disk electrodes, 1.0 mg of doped nanotubes were placed into a microvial followed by 100 μL of Nafion suspension. The mixture was mixed on a vortex mixer for 1 min followed by sonication in a sonic water bath for 1 min, and then placed on a vortex mixer for 1 min more. Twenty milliliters of the mixture was then immediately pipetted onto the glassy carbon rotating disk electrodes and spread across the entire surface including the Teflon insulation to ensure a uniformly adhered layer. The rotating ring disk electrodes were prepared in a similar fashion but used 2.0 μL of the suspension placed directly onto the glassy carbon disk with great care to keep the suspension from contacting the platinum ring. The electrodes were allowed to dry for 1 h on a countertop then soaked for 1 h in 1 M KOH. Rotating disk electrode voltammetry was performed at 4000 rpm in aerated 1 M KOH with a platinum counter and a Hg/HgO reference electrode. Rotating ring disk electrode voltammetry was performed in a similar setup but only rotated at 3000 rpm due to the manufacturer imposed limitation of the electrode. The rotating disk electrodes that were used were Pine Instruments model AFE2M050GC and the rotating ring disk electrodes were model AFE7R9GCPT with a 37% collection efficiency. The rotator used for the experiments was Pine Instruments model AFM-SRX, and the electrochemical measurements for rotating disk electrodes were taken by a CH Instruments model 620 potentiostat interfaced to a PC. The RRDE measurements were taken with a CH Instruments model 1030 potentiostat because the RRDE experiments required a bipotentiostat. The XPS spectra were acquired at Kratos AXIS ULTRA X-ray photoelectron spectrometer using monochromatic Al Kα source operating at 300 W. The operating pressure was 3×10^{-9} Torr. Charge neutralization using low energy electrons was used for charge compensation, Following a survey of each area is the recording of high-resolution spectra of C 1s, O 1s, N 1s, and Co 2p or Fe 2p depending on sample. A linear background was used for quantifying the C, O, and N spectra and Shirley background for quantifying Co and Fe spectra. All the spectra were charge referenced to the aliphatic carbon at 284.8 eV. Individual peaks of constrained width, position and 70% Gaussian/30% Lorentzian line shape were used for curve fitting. The widths of peaks in the curve-fit of C 1s, N1s, and Co2p/Fe2p were set to be 1.0, 1.0, and 1.4 eV respectively.

RESULTS AND DISCUSSION

After nanotube synthesis, the cleaned dry carbon nanotubes were characterized with electron microscopy. The carbon nanotubes produced with just hexane (solvent), iron powder (growth catalysts/chlorine scavenger), and carbon tetrachloride (carbon source) were very straight and large multiwalled carbon nanotubes, with an average length of 1.161 $\pm$ 0.190 μm, average widths of 118 $\pm$ 17 nm, and wall thicknesses of 33 $\pm$ 9 nm. A transmission electron micrograph is shown in Figure 1. The nanotubes have smooth walls and have closed ends. The nanotubes made with the addition of cobaltocene, which is a growth initiator for carbon nanotubes, had a very different morphology than the nanotubes synthesized without it. Figure 2 shows a transmission electron micrograph of these nanotubes. These nanotubes had a very diverse wormy morphology with imperfections in the walls and many branching points. The average length was 2.348 $\pm$ 1.238 μm, the average width was 143 $\pm$ 91 nm, and the average wall thickness was 60 $\pm$ 39 nm. The phthalocyanine doped carbon nanotubes had a very different structure that the previously synthesized

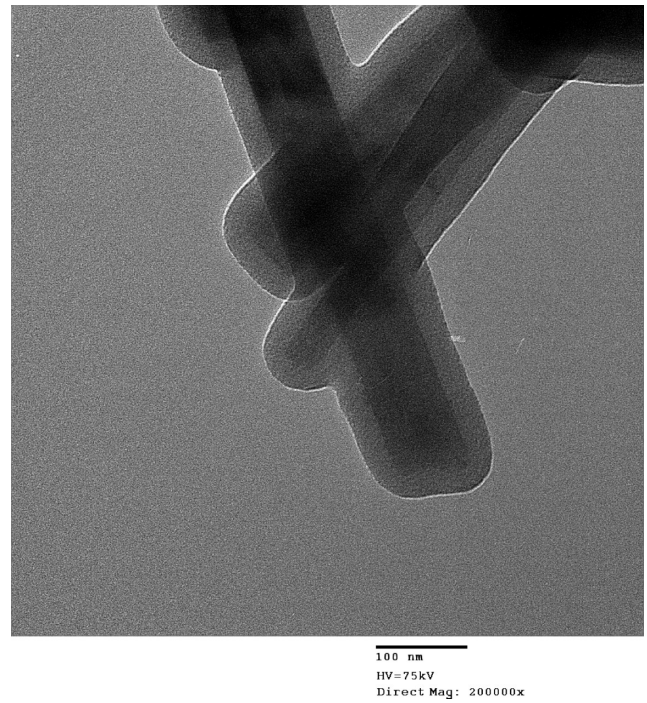

FIGURE 1. Transmission electron micrograph of multiwalled carbon nanotubes synthesized in critical point hexane with iron and carbon tetrachloride.

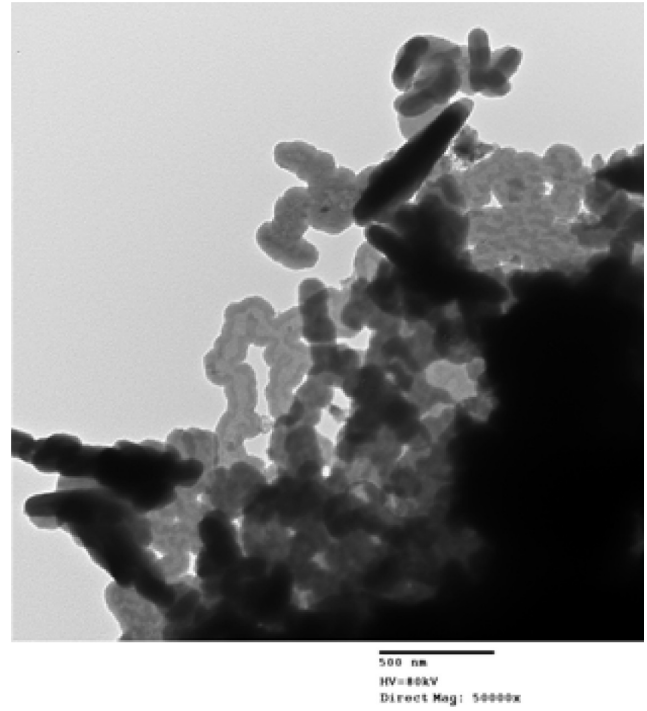

FIGURE 2. Transmission electron micrograph of carbon nanotubes synthesized with additional cobaltocene growth catalyst.

nanotubes without dopant. The size of these nanotubes was diverse with average widths of 255 $\pm$ 87 nm and average lengths of 7.300 $\pm$ 2.162 μm. Scanning electron microscopy showed that the doped nanotubes were very linear without any bends or curls, as shown in Figure 3. The TEM image of the phthalocyanine doped carbon nanotubes in Figure 4 shows that they maintain the tubular structure similar to the nanotubes synthesized with only iron metal and carbon

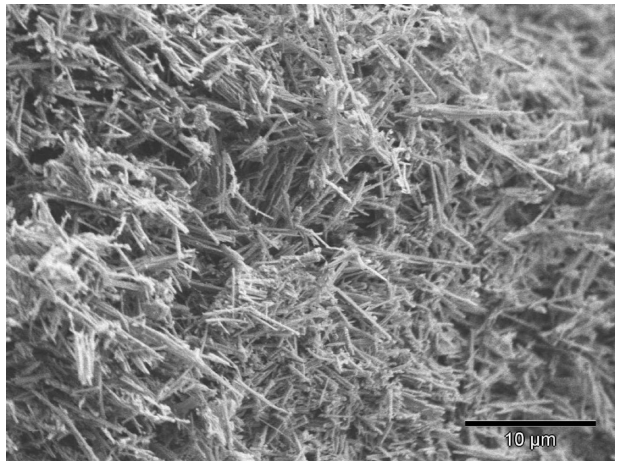

FIGURE 3. Scanning electron micrograph of phthalocyanine-doped nanotubes.

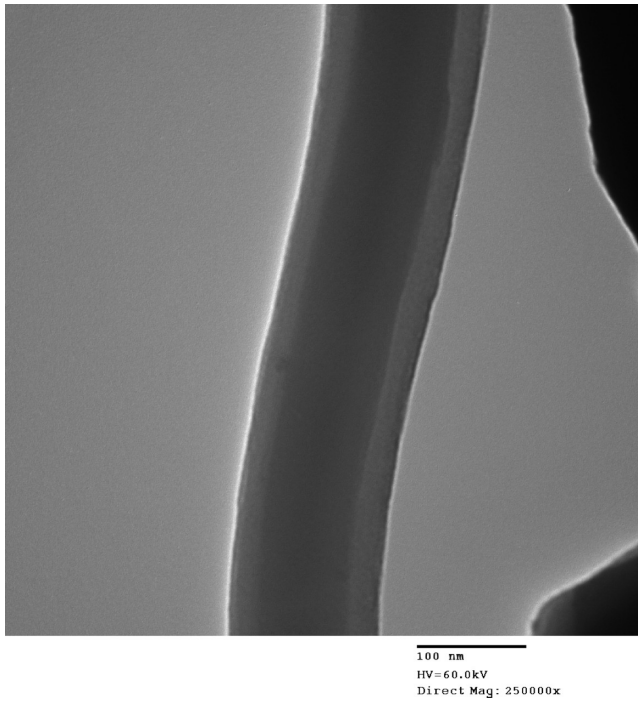

FIGURE 4. Transmission electron micrograph of phthalocyanine-doped carbon nanotubes.

tetrachloride. The wall average thickness from TEM was determined to be 21 ± 8 nm for the phthalocyanine-doped nanotubes.

The electrochemistry of the phthalocyanine doped carbon nanotubes was characterized by rotating disk electrode voltammetry. The iron phthalocyanine doped nanotubes showed a half wave oxygen reduction potential of −0.210 ± 0.008 V vs Hg\HgO (Hg\HgO has a reference potential of 0.140 V vs NHE). The half wave reduction potential is determined by the midpoint between the onset of reduction and the maximal steady state value of reduction. The cobalt phthalocyanine-doped carbon nanotubes showed a half wave oxygen reduction potential of −0.050 ± 0.005 V vs Hg\HgO. Figure 5 shows representative voltammograms comparing both catalytic materials. Platinum's oxygen reduction potential was also determined in the same alkaline

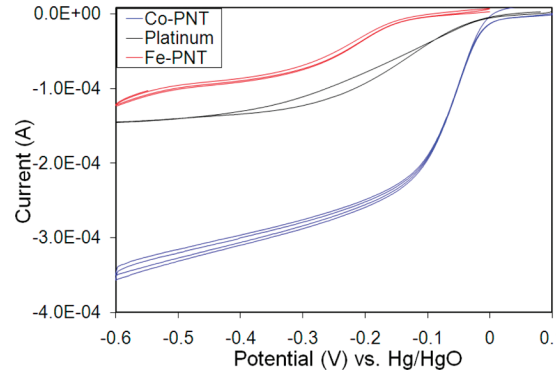

FIGURE 5. Representative rotating disk voltammograms for iron phthalocyanine-doped nanotubes (red) and cobalt phthalocyanine doped nanotubes (blue). Electrodes were rotated at 4000 rpm in air saturated 1 M KOH solution with platinum counter electrodes and Hg\HgO reference electrodes.

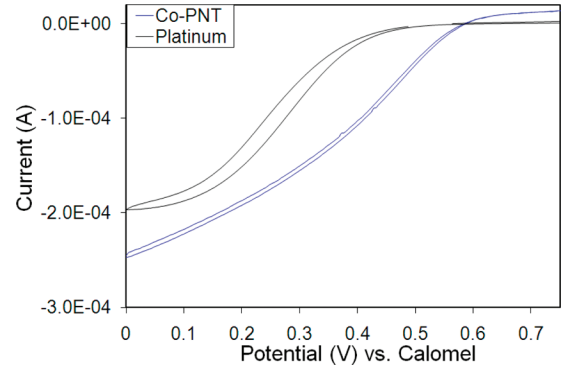

FIGURE 6. Representative rotating disk voltammograms for cobalt phthalocyanine doped nanotubes (blue) and platinum in 1 M H_2SO_4 vs calomel. Electrodes were rotated at 4000 rpm in air saturated solution with platinum counter electrodes.

media. Its half wave reduction potential was determined to be −0.197 ± 0.002 V vs Hg\HgO. In comparison to platinum the, iron phthalocyanine-doped nanotubes reduce oxygen with 12 mV more overpotential than platinum, making them a reasonable alternative catalyst to platinum. However, the cobalt phthalocyanine doped nanotubes were able to reduce oxygen at 147 mV less overpotential than platinum making them a superior alternative catalyst to platinum from a purely kinetic point of view. When this is considered along with the resistance to passivation that has been reported for other chelated cobalt catalysts, this is a superior catalytic material compared to platinum (18). Clearly the cobalt doped material required less overpotential to achieve oxygen reduction than the iron doped material which has also been observed with other chelated cobalt and chelated iron catalysts (18). Comparative RDE voltammograms were also performed on the cobalt doped material and platinum in acidic media to demonstrate that the catalytic oxygen reduction still maintains the same chemistry seen in literature with cobalt porphyrins and phthalocyanines shown in Figure 6. Rotating ring disk electrode (RRDE) voltammetry was performed on the cobalt exchanged phthalocyanine doped carbon nanotubes to further confirm that oxygen reduction was taking place. The ring was held at +0.5 V to be consistent with literature procedures (25). The RRDE voltammogram shown in Figure 7 indicate that both two electron

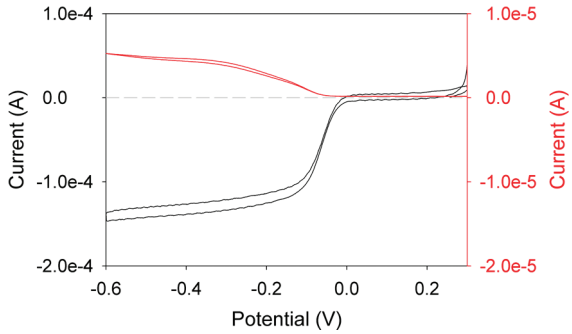

FIGURE 7. Representative RRDE voltammogram for cobalt exchanged phthalocyanine doped nanotubes showing oxygen reduction at the CO-PNT modified disk (black) and oxidation at the ring (red). This was taken with a rotation rate of 3000 rpm in 1 M KOH with a pt counter and Hg\HgO reference electrode. The Pt ring was biased at +0.5 V while the disk potential was scanned at 0.001 V\S.

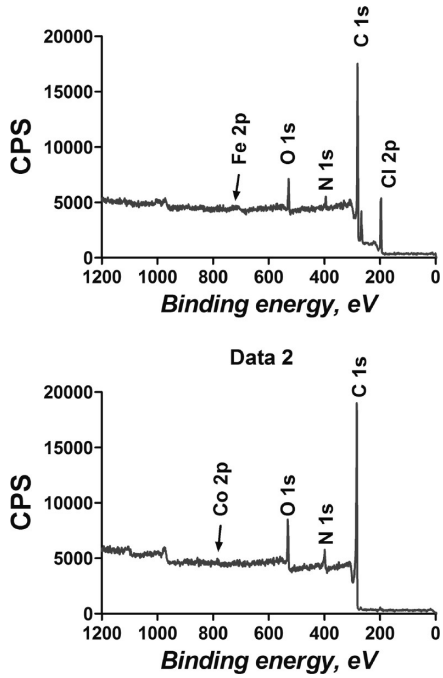

FIGURE 8. Low-resolution survey spectra showing the elemental composition of the iron phthalocyanine doped nanotubes (top) and cobalt phthalocyanine-doped nanotubes (bottom).

oxygen reduction to peroxide and four electron oxygen reduction to water are occurring. Since the collection efficiency of the Pt ring is 37%, this would indicate that when the disk reaches steady-state current at −0.150 V that the majority of oxygen is being reduced to water. In Figure 7, the disk current at a potential of −0.150 V is 1.191×10^{-4} A. Because the ring current was 2.074×10^{-6} A and the collection efficiency was 37%, this means that 95.3% of the current passed reduces oxygen to water and 4.7% of the current reduces oxygen to peroxide. The peroxide generated is detectable at the platinum ring as an oxidation back to molecular oxygen. These results indicate that the cobalt exchanged phthalocyanine doped nanotubes exhibit similar chemistry as other cobalt phthalocyanine compounds (20, 21), but maintain different material properties than other phthalocyanine based catalysts which is advantageous, because the material properties of the other phthalocyanine catalysts

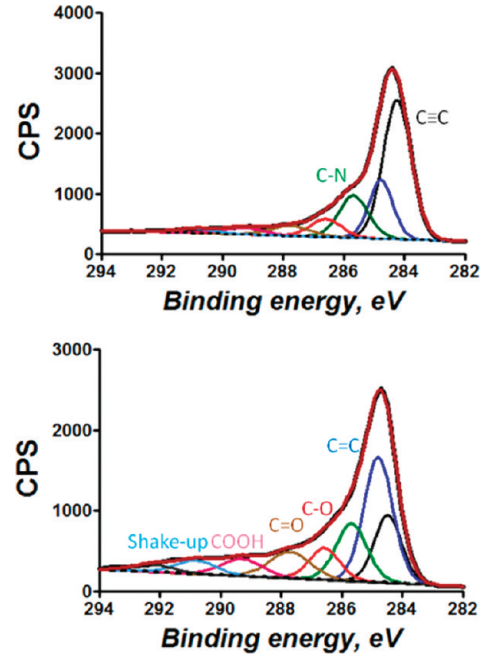

FIGURE 9. X-ray photoelectron spectrum for C1s of Fe-PNT (top) and Co-PNT (bottom).

Table 1. Elemental Analysis of Phthalocyanine-Doped Nanotubes with Iron and Cobalt

	% carbon	% oxygen	% nitrogen	% iron	% cobalt
Fe-PNT	90.8	5.8	3.1	0.37	
Co-PNT	87.4	6.2	6.0		0.43

limit their applications. The other advantage is that these doped nanotubes can be used in the same way as conventional Pt\C type catalysts, because the catalyst formed is a conductive powder. Another advantage of cobalt phthalocyanines and cobalt porphyrins is their ability to reduce oxygen in both alkaline media and acidic media similar to platinum (26). Many catalysts are able to reduce oxygen in alkaline media, but few exhibit the ability to both (27). This makes the cobalt phthalocyanine doped nanotubes good for oxygen reduction in low-temperature proton exchange fuel cells.

XPS was performed on both the iron phthalocyanine doped nanotubes and the cobalt phthalocyanine doped nanotubes to get a more full understanding of the surface composition and what types of moieties exist in these new types of materials. Low resolution survey spectra and elemental composition of the phthalocyanine doped nanotubes are shown in Figure 8 and Table 1. Iron phthalocyanine doped nanotubes have Cl contamination most likely due to incomplete reaction of chlorocarbon starting materials, but the Cl peak disappears after further heat treatment with the molten cobalt chloride. The Cl peak was excluded from the total elemental composition for adequate comparison between samples. Table 1 indicates that the relative percentages of each element shifted slightly from the iron doped sample and the cobalt doped sample, most likely due to the cobalt exchanging process. The backbone of the starting material is 78.0% carbon, 19.5% nitrogen, and

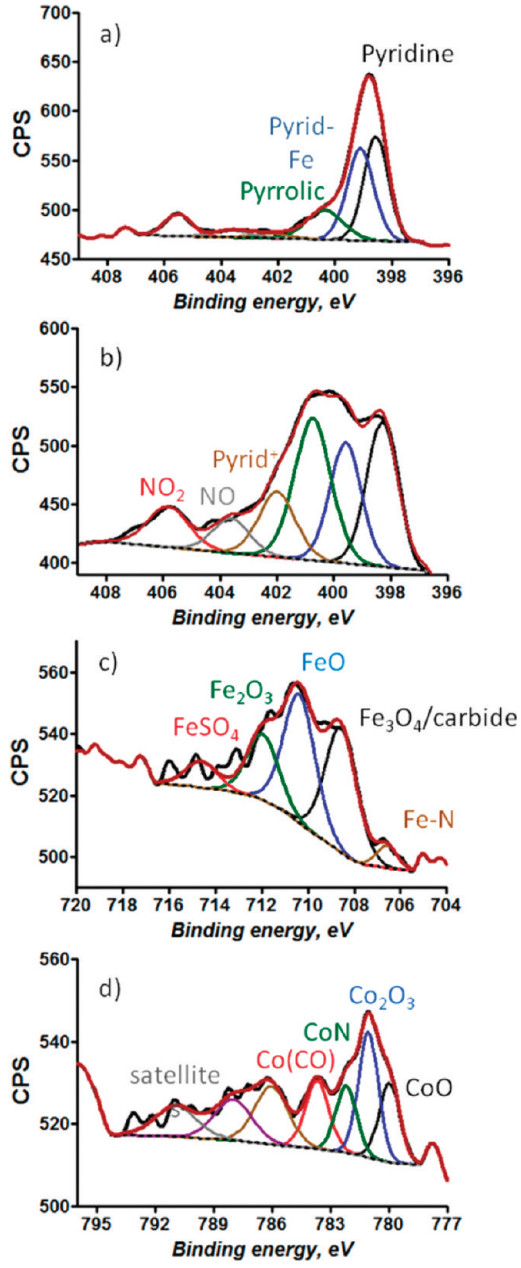

FIGURE 10. N1s XPS spectrum for phthalocyanine doped nanotubes that contain (a) chelated iron and (b) chelated cobalt. (c) Fe 2p spectrum for chelated iron and (d) Co 2p for chelated cobalt.

2.5% iron. The increase in the percentage of carbon between the starting material and the nanotube material is what was to be expected, because there is an addition of carbon tetrachloride to the synthesis to form the graphene sheets that the phthalocyanines get incorporated into. The ratio of nitrogen to metal remains constant for the starting material and the doped nanotube material indicating that the nanotube synthesis allows the nitrogen to remain in the final structure. This is also a strong indication that the phthalocyanine backbone gets incorporated wholly into the final nanotube structure without rearrangement or damage. The representative XPS C1s spectra for both iron and cobalt doped nanotubes is shown in Figure 9. Initial inspection shows that both samples contain large quantities of sp2-hybridized carbon, followed by the next-highest contributor

Table 2. XPS Deconvolution Results Indicating the Relative Percent of Each Type of Bond Detected in the Spectrum

binding energy (eV)	bond type	Fe-PNT (%)	Co-PNT (%)
284.3	C≡C	42.1	17.5
284.8	C═C	17.5	26.8
285.7	C−N	14.7	15.1
286.6	C−O	6.2	7.6
287.7	N−C−O, N−C═O, C═O	5.2	8.5
289.3	COOH	3.0	5.5
398.4	N-pyridyl	0.9	1.4
399.4	metal-N-pyridyl	1.2	1.2
400.6	pyrrolic amine	0.4	1.6
402.0	pyridyl+	0.1	0.7
403.5	pyridyl oxide/graphitic	0.1	0.5
405.7	NO_2-	0.4	0.7
	C shakeup, O 1s, Fe 2p	8.4	13.1
	total bond signal	100	100

of nitrogen−carbon moieties, and finally some oxygen-containing moieties that would be expected to be present because of the oxidative cleaning procedure after the synthesis. The N1s XPS spectrum shown in Figure 10 was curve-fitted using 6 symmetrical peaks having the same full-width half-maximum (fwhm). Following peak assignment was done based on data reported in literature (28−30) and reference databases (31): peak at 398.4 ± 0.2 eV is pyridyl N, peak at 399.4 ± 0.2 eV is pyridyl N associated with metal, peak at 400.6 ± 0.2 eV is pyrrolic N, peak at 402 ± 0.2 eV is pyridyl$^+$, peak at 403.5 ± 0.2 eV is reported to be graphitic and N oxide, and peak at 405.7 ± 0.2 eV is due to NO_2^-. Large range of binding energies for pyridyl N is reported in the literature -from 398.2 to 399 eV. We can see that pyridyl N for iron-chelated sample is detected at 398.6 eV, while that for cobalt-chelated samples is detected at 398.2 eV. Shift in binding energy of pyridyl N bound to metal has been reported in the literature causing this peak to shift to ~399.2 eV (29, 30). Moreover, we have analyzed Fe phthalocyanine (unpyrolyzed) for reference and found the same binding energy of N 1s peak that is associated with metal. Identification of this peak is also confirmed by peak detected in high-resolution spectra of both metals due to association with nitrogen as discussed below.

N 1s spectra indicate that there is almost twice as much pyrrolic N (400.6 eV) in the cobalt chelated phthalocyanine doped nanotubes compared to the iron-doped phthalocyanine doped nanotubes. This indicated that two phenomena occurred, one that the phthalocyanine backbone retained the nitrogen moieties during the synthesis, and that the extreme heating during the cobalt metal exchange altered the pyridyl N (398.4 eV) converting some of it to a pyrrolic N (400.6 eV). Figure 10 shows Co2p and the Fe2p high resolution spectra that were deconvolved into multiple peaks. Peak assignment is based on reference database, reported literature and reference materials, such as Fe and Co oxides and Fe phthalocianene analyzed by XPS (28, 30, 32). High resolution spectra show that there is chelated metal and that the cobalt was successfully exchanged in the doped

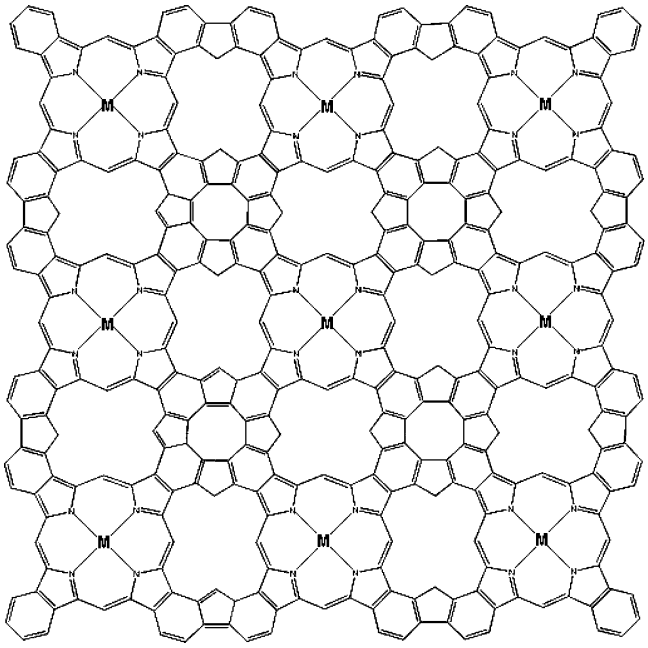

FIGURE 11. One possible graphitic type structure that agrees with the elemental analysis of the phthalocyanine-doped nanotubes.

nanotubes replacing the iron and that there is a lot of bound oxygen to the chelated metals, which is to be expected for catalysts that reduce oxygen. Both spectra have peaks due to metal associated with N (peak 706.6 eV for Fe 2p and 782.1 for Co 2p), affirming peak detected in N 1s spectrum due to association with metal. The Fe2p XPS spectrum in Figure 10c also shows that there is iron carbide (708.6 eV) that exists in the iron-containing nanotube samples. This suggests that iron carbide is an important intermediate product of the reaction that forms graphene for the doped nanotubes. This has also been observed with other methods of making carbon nanotubes (33, 34), indicating that our growth mechanism is similar. The overall deconvolution of the XPS spectrum is shown in Table 2. These data suggest that the material is graphitic in nature with a large percentage of aromatic nitrogen moieties that are capable of chelating transition metals. This material is very versatile, because not only is it conductive but it has the ability to be tailored for a specific types of catalysis by exchanging one catalytic metal center for another. Figures 11 and 12 are two possible graphitic type structures that are in agreement with the elemental analysis results. These are somewhat similar to

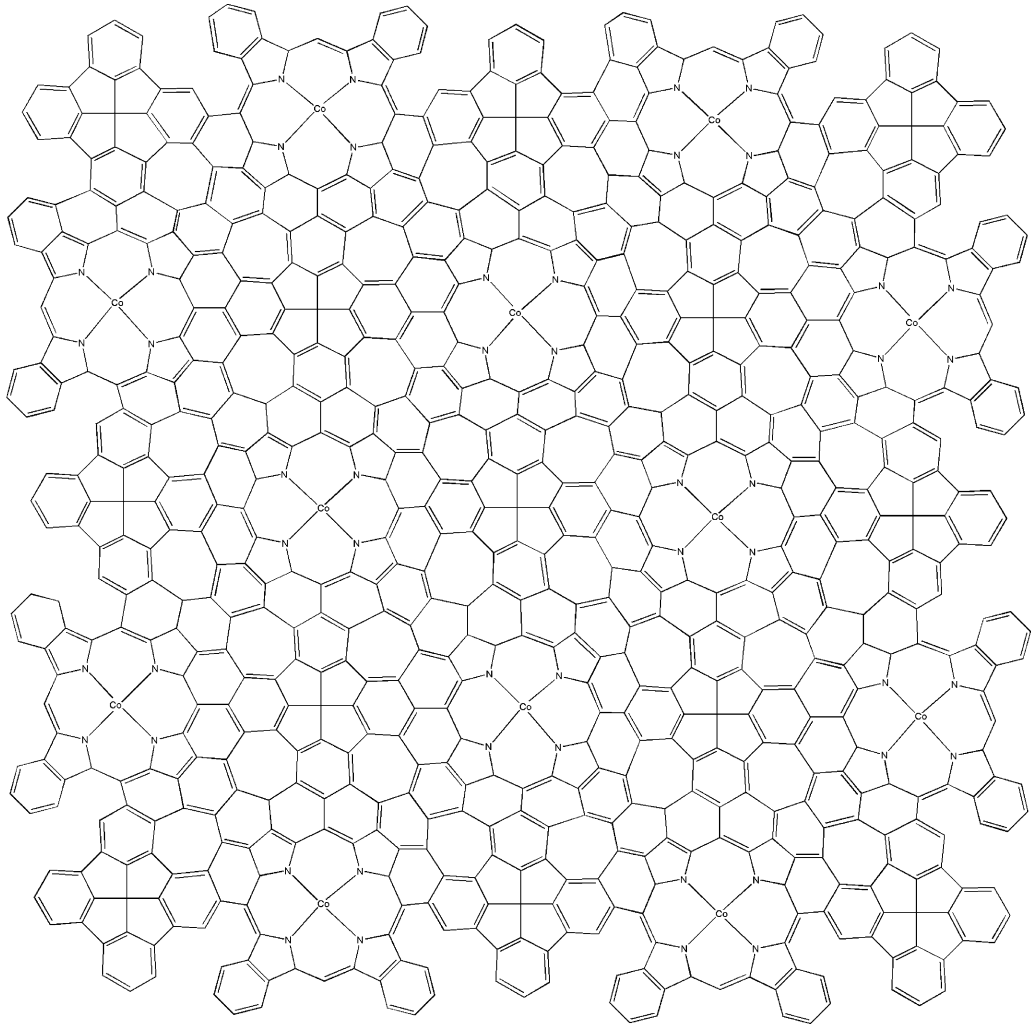

FIGURE 12. Another possible graphitic type structure for the phthalocyanine dope nanotubes that agrees with the elemental analysis that contains a higher ratio of carbon to nitrogen.

what has been proposed for pyrolized cobalt porphyrin, which also has a graphitic nature (35).

CONCLUSIONS

By developing a bulk low-temperature critical point solvent synthesis method of growing carbon nanotubes, it became possible to incorporate the phthalocyanines into the growing nanotubes giving a final material the catalytic properties of the phthalocyanine. The XPS data that was taken supports that the phthalocyanine backbone and pyrrolic amine remain in the final material, similar to porphyrin pyropolymers (18, 35). The synthesis that was developed, which is a halocarbon reduction by metallic iron, is very versatile, allowing reduction of both halogenated alkanes and halogenated aromatics. It also is very tunable; by introduction of a carbon nanotube growth catalyst, the nanotubes can be grown with different morphologies.

The phthalocyanine- doped nanotubes that were originally iron-containing showed oxygen reduction, but at overpotentials that would make it not competitive enough with platinum. To change this, the iron was exchanged for cobalt in a simple molten cobalt salt slurry which yielded a catalytic material that displayed the catalytic properties of cobalt phthalocyanine. The RRDE and RDE supported that this cobalt doped material was superior to the iron doped material and platinum. The cobalt material also displays oxygen reduction chemistry in acidic media, which means that this would have utility as a replacement for platinum catalysts in acidic and alkaline media. This ability to swap metals for different chemistry makes this material versatile, not only as a fuel cell catalyst but as a catalyst for any number of reactions that require a metal chelate or a chelated electrocatalyst. This could yield a non-platinum-catalyzed fuel cell with good performance.

Acknowledgment. The authors thank the National Science Foundation for funding.

REFERENCES AND NOTES

(1) Mukerjee, S.; Lee, S. J.; Ticianelli, E. A.; McBreen, J.; Grgur, B. N.; Markovic, N. M.; Ross, P. N.; Giallombardo, J. R.; De Castro, E. S. *J. Electrochem. Soc.* **1999**, *2*, 12.
(2) Igarashi, H.; Fujino, T.; Zhu, Y.; Uchida, H.; Watanabe, M. *Phys. Chem. Chem. Phys.* **2001**, *3*, 306.
(3) Minteer, S. D.; Liaw, B. Y.; Cooney, M. J. *Curr. Opin. Biotechnol.* **2007**, *18*, 228.
(4) Stamenkovic, V. R.; Fowler, B.; Mun, B. S.; Wang, G.; Ross, P. N.; Lucas, C. A.; Markovic, N. M. *Science* **2007**, *315*, 493.
(5) Anderson, A. B.; Grantscharova, E.; Seong, S. *J. Electrochem. Soc.* **1996**, *143*, 2075.
(6) Schmidt, T. J.; Noeske, M.; Gasteiger, H. A.; Behm, R. J.; Britz, P.; Bonnemann, H. *J. Electrochem. Soc.* **1998**, *145*, 925.
(7) Koper, M. T. M.; Shubina, T. E.; van Santen, R. A. *J. Phys. Chem. B* **2002**, *106*, 686.
(8) Roth, C.; Benker, N.; Zils, S.; Chenitz, R.; Issanin, A.; Fuess, H. *Oldenbourg* **2007**, *221*, 1549.
(9) Matsushita, K.; Yakaushi, T.; Toyama, H.; Shinagawa, E.; Adachi, O. *J. Biol. Chem.* **1996**, *271*, 4850.
(10) Ferapontova, E. E.; Gorton, L. *Bioelectrochemistry* **2005**, *66*, 55.
(11) Shleev, S.; Tkac, J.; Christenson, A.; Ruzgas, T.; Yaropolov, A. I.; Whittaker, J. W.; Gorton, L. *Biosens. Bioelectron.* **2005**, *20*, 2517.
(12) Wu, Y.; Shen, Q.; Hu, S. *Anal. Chim. Acta* **2006**, *558*, 179.
(13) Whittaker, M. M.; Pan, H.; Yukl, E. T.; Whittaker, J. W. *J. Biol. Chem.* **2007**, *282*, 7011.
(14) Su, L.; Kelly, J. M.; Hawkridge, F. M. *Electrochem. Soc. Trans.* **2007**, *2*, 1.
(15) Yang, R.; Bonakdarpour, A.; Easton, E. B.; Stoffyn-Egli, P.; Dahn, J. R. *J. Electrochem. Soc.* **2007**, *154*, 275.
(16) Lefèvre, M.; Proietti, E.; Jaouen, F.; Dodelet, J.-P. *Science* **2009**, *324*, 71.
(17) Okada, T.; Katou, K.; Hirose, T.; Yuasa, M.; Sekine, I. *J. Electrochem. Soc.* **1999**, *146*, 2562.
(18) Artyushkova, K.; Levendosky, S.; Atanassov, P.; Fulghum, J. *Top. Catal.* **2007**, *43*, 263.
(19) Okada, T.; Gokita, M.; Yuasa, M.; Sekine, I. *J. Electrochem. Soc.* **1998**, *145*, 815.
(20) Song, E.; Shi, C.; Anson, F. C. *Langmuir* **1998**, *14*, 4315.
(21) Choi, A.; Jeong, H.; Kim, S.; Jo, S.; Jeon, S. *Electrochim. Acta* **2008**, *53*, 2579.
(22) Shaijumon, M. M.; Ramaprabhu, S. *Chem. Phys. Lett.* **2003**, *374*, 513.
(23) Kawasaki, S.; Shinoda, M.; Iwai, Y.; Ogawa, M.; Hara, T.; Hattori, Y.; Kubota, T. *Solid State Commun.* **2006**, *138*, 382.
(24) Lee, D. C.; Mikulec, F. V.; Korgel, B. A. *J. Am. Chem. Soc.* **2004**, *126*, 4951.
(25) Antoine, O.; Durand, R. *J. Appl. Electrochem.* **2000**, *30*, 839.
(26) Zhao, F.; Harnisch, F.; Schröder, U.; Scholz, F.; Bogdanoff, P.; Herrmann, I. *Environ. Sci. Technol.* **2006**, *40*, 5193.
(27) Kinoshita, K. *Electrochemical Oxygen Technology*; John Wiley and Sons: Danvers, ME, 1992.
(28) Jaouen, F.; Herranz, J.; Lefevre, M.; Dodelet, J. P.; Kramm, U. I.; Herrmann, I.; Bogdanoff, P.; Maruyama, J.; Nagaoka, T.; Garsuch, A.; Dahn, J. R.; Olson, T.; Pylypenko, S.; Atanassov, P.; Ustinov, E. A. *ACS Appl. Mater. Interfaces* **2009**, *1*, 1623.
(29) Olson, T. S.; Pylypenko, S.; Fulghum, J. E.; Atanassov, P. *J. Electrochem. Soc.* **2010**, *157*, B54.
(30) Artyushkova, K.; Pylypenko, S.; Olson, T. S.; Fulghum, J. E.; Atanassov, P. *Langmuir* **2008**, *24*, 9082.
(31) *NIST X-ray Photoelectron Spectroscopy Database*; National Institute for Standards and Technology: Gaithersburg, MD.
(32) *Handbook of XPS*; Physical Electronics Corporation: Chanhassen, MN, 1992.
(33) Yoshida, H.; Takeda, S.; Uchiyama, T.; Kohno, H.; Homma, Y. *Nano Lett.* **2006**, *8*, 2082.
(34) Schaper, A. K.; Hou, H.; Greiner, A.; Phillipp, F. *J. Catal.* **2004**, *222*, 250.
(35) Ziegelbauer, J. M.; Olson, T. S.; Pylypenko, S.; Alamgir, F.; Jaye, J.; Atanassov, P.; Mukerjee, S. *J. Phys. Chem.* **2008**, *112*, 8839.

AM100724V